

Reliable density functional and G_0W_0 approaches to the calculation of bandgaps in 2D materials.

Musen Li,^{1,2} Michael J. Ford,² Rika Kobayashi,³ Roger D. Amos² and Jeffrey R. Reimers^{1,2}

1 International Centre for Quantum and Molecular Structures and Department of Physics, Shanghai University, Shanghai 200444, China.

2 University of Technology Sydney, School of Mathematical and Physical Sciences, Ultimo, New South Wales 2007, Australia.

3 ANU Supercomputer Facility, Leonard Huxley Bldg. 56, Mills Rd, Canberra, ACT, 2601, Australia.

Email: jeffrey.reimers@uts.edu.au

ABSTRACT Optimizing density-functional theory (DFT) and G_0W_0 calculations present coupled problems as orbitals from DFT are needed as G_0W_0 starting points. Applied to 341 two-dimensional (2D) materials, we demonstrate that CAM-B3LYP provides minimal changes in bandgap (e.g., mean absolute deviation of 0.23 eV) when used to start G_0W_0 calculations, compared to traditional functionals such as PBE, PBE0, and HSE06 (1.07 eV, 1.48 eV, and 1.51 eV, respectively). CAM-B3LYP also delivers the smallest changes in orbital representation. These and other results indicate the suitability of CAM-B3LYP as a density-functional approach for modelling 2D materials, as well as for use in optimizing G_0W_0 calculations. Our findings parallel well established features of applications to molecules, as well as for spectroscopic applications involving 3D materials.

Two-dimensional (2D) materials sparked widespread research, owing to their attractive electronic, photonic, and straintronic characteristics [1, 2] and distinctive spintronic and optoelectronic quantum features [3, 4]. They show great promise and provide numerous opportunities in related fields such as catalysis, hybrids energy storage solar cells, and ultrathin devices [5]. In addition to properties that differ from conventional bulk or surface materials, the distinctive manipulability of 2D materials by mechanics [6, 7], light [8], electric field [1], and magnetic field [9] have further expanded the prospects for 2D materials applications. At the same time, many 2D materials have been prepared by tailored preparation methods, driving research in areas such as low-dimensional devices [7, 10].

Among the many applications of 2D materials, band-structure engineering is an important one that plays a vital role in optoelectronics [8, 11, 12], catalysis [13], communications [14-16], photoluminescence emitters [7] and sensors [17]. From black phosphorus to monolayer hexagonal boron nitride (h-BN), 2D semiconductors can show highly tunable bandgaps produced, e.g., by alloying [18], doping [19, 20], and adding defects [21].

As the chemical and structural properties of 2D materials can be very different to 3D ones, and as intuition concerning the optical properties of 2D materials may be difficult to estimate from known properties of 3D materials owing to the significant difference in dielectric properties [22], accurate first-principles simulation methods are required to boost 2D material design and data interpretation [10]. Considered herein are applications of density-functional theory (DFT) [23] and *ab initio* Green's function theory implemented at the G_0W_0 level [24].

As a most effective first-principles method, DFT has had widespread use for the modelling and design of both molecular systems and bulk materials. Nevertheless, the precise exchange-correlation functional of DFT is unknown, and in all postulated functionals, the exchange component of DFT has a different asymptotic shape compared to the Coulomb term. As a result, these DFT functionals manifest flaws, such as self-interaction errors and errors associated with charge partial occupancy [25]. These problems can lead to a less-than-

accurate description of the electronic structure that significantly impacts on properties such as the bandgap, spectral transition energies, exciton binding strengths, and spectral assignment [26-30]. To improve the description of electron exchange, hybrid DFT methods such as B3LYP [31, 32], PBE0 [33], and HSE06 [34] have been developed. For materials, HSE06 proved successful for the description of metals and important semiconductors such as silicon [35-38], with this success owing to the functional-design criteria and the lack of internal charge transfer in these systems. Further, HSE06 is currently perceived as being the best widely-available functional for the evaluation of materials spectroscopic properties [39], giving results generally superior to those from generalized-gradient approximation (GGA) functions such as PBE [40] and its many variants.

Despite significant achievements, the performance of most known functionals, including HSE06 and PBE0, actually remains poor for general 3D materials [24, 29, 30]. For them, mean absolute error compared to experiment for bandgap calculations of 3D materials has been recorded in the range of 0.5 – 0.8 eV [29, 39], making them unsuitable for choosing between multiple possible experimental spectroscopic data assignments. General issues involve the failure of most functionals to properly separate charge, their incorrect representation of the dielectric constant, and its neglect of dispersion forces. These three effects are related, yet usually treated differently during density-functional design. Additional corrections such as D3 [41] are often added to empirically account for dispersion, whereas the charge-separation and dielectric-constant issues have been the subject of numerous recent DFT developments [29, 30, 35-37, 42-44].

Practical solutions to the charge-separation problem alone have been known for two decades, with many approaches now in common use. This work follows advances [45, 46] associated with the development of the CAM-B3LYP density functional [47]. Recently, CAM-B3LYP has become available [29, 30, 43] to materials simulations, driving significant improvement in the simulation of spectroscopic properties of 3D insulators and semiconductors [29].

Methods like CAM-B3LYP are essential for the understanding of the spectroscopy of large aromatic molecules [43, 48, 49], including photosystems [50-52], and the difference in dielectric properties between 2D and 3D materials [22] suggests that its influence on 2D simulations will be profound. For defects in h-BN, CAM-B3LYP has already been shown to be able to usefully evaluate excited-state energies of widely varying types to order spectroscopic transitions and facilitate experimental assignment, applications for which HSE06 was found to be inadequate [29, 53]. It has also been shown to give results similar to *ab initio* approaches to defect spectroscopic simulations [53].

As an alternative to DFT, *ab initio* approaches using the G_0W_0 [24] approximation, in general, provide significantly improved accuracy but at much higher computational cost [54]. For periodic materials, this method computes quasiparticle energies from a single GW iteration by disregarding all off-diagonal matrix members of the self-energy [55]. It provides a non-interaction Green's function and screened-Coulomb interaction convolution, expanded around the band energies given by some prior DFT calculation. Unfortunately, the results obtained depend strongly on the quality of the DFT method used to provide the initial wavefunction [56, 57]. If the electronic distribution presented in the prior DFT calculation is good, then G_0W_0 will introduce only minor corrections, whereas if the prior DFT calculations are poor, then the G_0W_0 corrections will be large and a qualitatively realistic solution may not necessarily be obtained [54].

Finding the most suitable density functional for some application, and optimizing the results of G_0W_0 calculations, therefore present as coupled problems [44, 58-61]. CAM-B3LYP has long been recognized as an optimal starting point for G_0W_0 calculations on molecules. For ionization energies, this conclusion arises from a study of 34 molecules using 10 density functionals [58], as well as a study of 100 molecules using 55 density functionals [61]. In the larger study, a mean deviation (MD) of 0.05 eV and a mean absolute deviation (MAD) of 0.24 eV were reported for CAM-B3LYP, compared, e.g., to much less useful results

for other approaches such as PBE (-0.57 eV and 0.61 eV), SCAN [62] (-0.48 eV and 0.54 eV), HSE06 (-0.30 eV and 0.37 eV) and PBE0 (-0.20 eV and 0.30 eV). Its performance for materials in general, and 2D materials in particular, therefore also needs to be further assessed. Supporting this, at the level of pure DFT, spectroscopic properties evaluated using CAM-B3LYP have already been demonstrated to provide substantial qualitative and quantitative improvements in the simulation of defects in hexagonal boron nitride (h-BN) compared to HSE06 [29, 53, 63-66].

CAM-B3LYP is chosen for study as it provides an example from amongst the numerous class of established density functionals that embody corrections to the asymptotic potential. Indeed, many related methods also appear worthy of similar investigation [29, 61], including those that correct for the dielectric constant that hold even more promise [35-37, 42, 67]. Of these approaches, one that has already been applied to enhance G_0W_0 calculations of specifically 3D materials is WOT-SRSH [67]. This functional delivers similar results to CAM-B3LYP in predicting bandgaps [29] and has been shown to provide significant improvements to G_0W_0 energies. Its current drawback is that it include internal parameters in the functional for which the values used are material-dependent and not clearly defined [44]. CAM-B3LYP is chosen herein as it provides an old and clearly established functional description that is universally applicable.

Two methods are widely used to postulate and screen 2D materials: (i) construction inspired by the properties of layered bulk materials, and (ii) brute-force construction by applying optimization algorithms based on atomic composition [68]. Many databases listing possible 2D materials have been created using these approaches, including C2DB [69] and MATHUB-2D [70]. In this work, 341 2D materials (see Supplemental Material) were chosen randomly for study from the C2DB database. The selected structures embody 53 elements and cover 26 different space groups, enough to make them suitable for usage as a benchmark data set.

All calculations were performed using the Vienna ab initio simulation package (VASP) [71, 72], using a customized version of VASP.6.3.2 that implements the CAM-B3LYP functional [30]. Self-consistent calculations are performed for the DFT and G_0W_0 band gaps using an energy-convergence criterion of 10^{-7} eV. The projector augmented wave (PAW) method [73] was used to describe the interactions between the valence electrons and the core electrons, with the contributions of the PAW sphere's non-spherical density gradients are taken into account. Standard “PBE” pseudopotentials [73] were not used as the shortcomings of CAM-B3LYP and G_0W_0 calculations are typically less than the shortcomings that these pseudopotentials provide [30]. Hence “GW” pseudopotentials, as specified in VASP POTCAR version 5.4, were used in all calculations. The plane-wave basis set kinetic energy cutoff is set to 500 eV to ensure the accuracy of the calculation; full details of the resulting basis set, plus the k -samplings used, are provided in Supplemental Material. The G_0W_0 calculations are performed using either CAM-B3LYP, PBE0, HSE06, or PBE starting orbitals; the results are named “ $G_0W_0@CAM-B3LYP$ ”, “ $G_0W_0@PBE0$ ”, “ $G_0W_0@HSE06$ ”, and “ $G_0W_0@PBE$ ”, respectively. Individually optimized atomic structures are obtained for each density functional, using a force convergence criterion of 10^{-3} eV Å⁻¹.

Full results, including optimized coordinates and calculated bandgaps for the 341 2D materials, are provided in Supplemental Material. Figure 1 compares the calculated $G_0W_0@PBE0$, $G_0W_0@HSE06$, and $G_0W_0@PBE$ bandgaps ΔE with those calculated by $G_0W_0@CAM-B3LYP$. Key statistical analyses are listed in Table I, including the mean differences (MD), mean average differences (MAD), the most negative differences, the most positive differences, the maximum absolute differences (MAX), and the maximum absolute percentage differences (MAPD). The bandgaps calculated starting with PBE0 orbitals and CAM-B3LYP orbitals are similar, with a MD of -0.12 eV, MAD of 0.14 eV, and MAX of 0.66 eV. In contrast, the differences to HSE06 results are ca. 3 times larger, with those to PBE results being up to 10 times larger. Supporting Material shows that the differences from $G_0W_0@HSE06$ and $G_0W_0@PBE$ results to $G_0W_0@PBE0$ ones are analogous.

A measure of the quality of the different G_0W_0 calculations is the quasiparticle weight [54, 74] Z obtained for the HOMO and LUMO orbitals. This measure is indicative of the similarity of the original orbitals to those as modified by the G_0W_0 procedure, with values near unity being desired. It has physical significance in that the HOMO band structures from G_0W_0 calculations typically display increased curvature compared to DFT band structures, indicating lower effective mass of the electrons in the material [54]. Results are listed in Table II for the minimum and average values of Z predicted for the 341 2D materials, with $G_0W_0@CAM-B3LYP$ providing the best results, $G_0W_0@PBE0$ being slightly poorer, and both $G_0W_0@HSE06$ and $G_0W_0@PBE$ providing significantly poorer results. Figure 1 shows the correlation between the $G_0W_0@CAM-B3LYP$ results and those from the other methods. Of interest, the treatments of the orbitals afforded by CAM-B3LYP and HSE06 appear to be similar, whereas those for PBE0 and PBE appear uncorrelated.

An alternative measure of quality is the change in the bandgap between that from a G_0W_0 calculation and that from its initiating DFT calculation, with results listed in Table I. CAM-B3LYP provides excellent results, realizing a MD of -0.19 eV, MAD of 0.23 eV, MAX of 0.53 eV, and MAPD of 7%. In contrast the changes introduced at the G_0W_0 level are 4-6 times larger for PBE0 and 6-8 times larger for G_0W_0 calculations starting with HSE06 or PBE orbitals.

Consideration of the pure-DFT bandgaps requires some standard to compare to, and in the absence of experimental data we choose $G_0W_0@CAM-B3LYP$ values as they are associated with the highest Z values and the smallest bandgap changes from pure DFT. Results from CAM-B3LYP, PBE0, HSE06, and PBE DFT calculations are compared to them in Figure 2 and Table I. The MD, MAD, MAX, and MAPD values range from 4-6 times larger for PBE0 to 6-10 times larger for HSE06 to 8-14 times larger for PBE.

A feature noted previously (Fig. 1) is the similarity of the CAM-B3LYP and HSE06 wavefunctions as indicated by the Z values manifested in the G_0W_0 calculations. To

investigate this, the overlaps between all occupied HSE06 and CAM-B3LYP DFT orbitals were computed, and indeed the calculated electron densities appear to be very similar. Overall, the results presented in the figures and tables perceive CAM-B3LYP to be highly accurate, PBE0 to be less accurate but viable, HSE06 to be of poor quality, and PBE to be highly unreliable, yet historically HSE06 has been the method of choice over PBE0 in materials spectroscopic simulations. Figure 1 suggests the possibility that it is the reliable qualitative nature of HSE06 orbitals, rather than the lower quantitative accuracy for bandgaps, that is the reason for this preference, as the impact of the orbital description influences most calculated materials properties.

In terms of qualitative features, an essential aspect of any DFT calculation is that it correctly determines the occupied orbitals. This property forms the basis of the empirical “DFT+U” scheme in which orbital forms are qualitatively retained and bandgaps adjusted to fit experiment. The G_0W_0 @PBE (etc.) calculations often reveal negative bandgaps, indicating that PBE actually failed to correctly describe the ground-state of the material. The serious underestimation of bandgaps predicted by PBE0, HSE06, and PBE (Fig. 2) leads to scenarios in which the predicted bandgap becomes less than the worst-case bandgap error for the method, and then even less than the average bandgap error for the method. When this happens, there is no guarantee that the method has correctly identified the ground state electronic structure, with results needing to be carefully considered. To illustrate this effect, Fig. 2 shows the cumulative band-gap-probability distributions obtained for the 341 2D materials using each DFT method, with the high-confidence region (bandgap above worst-case error) shaded in grey, the region of serious concern in which the bandgap is less than the average error shaded in pink, and the intermediate region shaded in green. There is a steady progression from CAM-B3LYP, for which only 2 of the 341 materials are in the intermediary region to PBE, for which most materials are in the region of serious concern, with PBE0 and then HSE06 intermediary.

Combined, the results for 341 2D materials indicate the high quality of the CAM-B3LYP DFT calculations and their suitability as starting orbitals for G_0W_0 calculations. Similar

results have already been observed for the application of CAM-B3LYP to G_0W_0 calculations of molecules [58, 61]. Also, the improvements found for the pure DFT results of CAM-B3LYP exceed the significant improvements already found [29, 61] compared to experiment for 3D materials (bandgap errors reduced by factors of: 1.8 for PBE0, 2.5 for HSE06, 3.7 for SCAN and 4-6 for PBE). In conclusion, for 2D materials (i) for CAM-B3LYP, the quality of the orbitals and energies is high, with G_0W_0 making minimal changes to both; (ii) for PBE0, the orbitals and energies are poorer, with G_0W_0 introducing adequate corrections; (iii) for HSE06, the orbitals are satisfactory but the energies poor and G_0W_0 does not result in quantitatively useful results, and (iv) for BPE, both orbitals and energies are very poor and hence the method is inappropriate for use in starting G_0W_0 calculations.

References:

1. P. Ranjan, S. Gaur, H. Yadav, A. B. Urgunde, V. Singh, A. Patel, K. Vishwakarma, D. Kalirawana, R. Gupta, and P. Kumar, *Nano Converg.* **9**, 26 (2022).
2. S. Manzeli, D. Ovchinnikov, D. Pasquier, O. V. Yazyev, and A. Kis, *Nat. Rev. Mater.* **2**, 17033 (2017).
3. X. Huang, C. Liu, and P. Zhou, *NPJ 2D Mater. Appl.* **6**, 51 (2022).
4. K. Ba, W. Jiang, J. Cheng, J. Bao, N. Xuan, Y. Sun, B. Liu, A. Xie, S. Wu, and Z. Sun, *Sci. Rep.* **7**, 45584 (2017).
5. Y. Ping, and T. J. Smart, *Nat. Comput. Sci.* **1**, 646 (2021).
6. K. Chen, J. Deng, Y. Yan, Q. Shi, T. Chang, X. Ding, J. Sun, S. Yang, and J. Z. Liu, *NPJ Comput. Mater.* **7**, 79 (2021).
7. D. Akinwande, C. Huyghebaert, C.-H. Wang, M. I. Serna, S. Goossens, L.-J. Li, H. S. P. Wong, and F. H. L. Koppens, *Nature* **573**, 507 (2019).
8. J. Jiang, Z. Chen, Y. Hu, Y. Xiang, L. Zhang, Y. Wang, G.-C. Wang, and J. Shi, *Nat. Nanotechnol.* **16**, 894 (2021).
9. K. S. Burch, D. Mandrus, and J.-G. Park, *Nature* **563**, 47 (2018).
10. M. C. Lemme, D. Akinwande, C. Huyghebaert, and C. Stampfer, *Nat. Commun.* **13**, 1392 (2022).
11. M. Bernardi, C. Ataca, M. Palummo, and J. C. Grossman, *Nanophotonics* **6**, 479 (2017).
12. A. Raja, A. Chaves, J. Yu, G. Arefe, H. M. Hill, A. F. Rigosi, T. C. Berkelbach, P. Nagler, C. Schüller, T. Korn, C. Nuckolls, J. Hone, L. E. Brus, T. F. Heinz, D. R. Reichman, and A. Chernikov, *Nat. Commun.* **8**, 15251 (2017).
13. C. Wang, R. Furlan de Oliveira, K. Jiang, Y. Zhao, N. Turetta, C. Ma, B. Han, H. Zhang, D. Tranca, X. Zhuang, L. Chi, A. Ciesielski, and P. Samorì, *Nat. Commun.* **13**, 510 (2022).
14. X. K. Cao, B. Clubine, J. H. Edgar, J. Y. Lin, and H. X. Jiang, *Appl. Phys. Lett.* **103**, 191106 (2013).

15. T.-A. Chen, C.-P. Chuu, C.-C. Tseng, C.-K. Wen, H. S. P. Wong, S. Pan, R. Li, T.-A. Chao, W.-C. Chueh, Y. Zhang, Q. Fu, B. I. Yakobson, W.-H. Chang, and L.-J. Li, *Nature* **579**, 219 (2020).
16. D. G. Smith, L. A. Burns, K. Patkowski, and C. D. Sherrill, *J. Phys. Chem. Lett.* **7**, 2197 (2016).
17. P. Ares, T. Cea, M. Holwill, Y. B. Wang, R. Roldán, F. Guinea, D. V. Andreeva, L. Fumagalli, K. S. Novoselov, and C. R. Woods, *Adv. Mater.* **32**, 1905504 (2020).
18. M. Kim, E. Pallecchi, R. Ge, X. Wu, G. Ducournau, J. C. Lee, H. Happy, and D. Akinwande, *Nat. Electron.* **3**, 479 (2020).
19. M. Kang, B. Kim, S. H. Ryu, S. W. Jung, J. Kim, L. Moreschini, C. Jozwiak, E. Rotenberg, A. Bostwick, and K. S. Kim, *Nano Lett.* **17**, 1610 (2017).
20. Y.-H. Chen, R. R. Tamming, K. Chen, Z. Zhang, F. Liu, Y. Zhang, J. M. Hodgkiss, R. J. Blaikie, B. Ding, and M. Qiu, *Nat. Commun.* **12**, 4332 (2021).
21. C. Chakraborty, K. M. Goodfellow, S. Dhara, A. Yoshimura, V. Meunier, and A. N. Vamivakas, *Nano Lett.* **17**, 2253 (2017).
22. P. Cudazzo, I. V. Tokatly, and A. Rubio, *Phys. Rev. B* **84**, 085406 (2011).
23. W. Kohn, and L. J. Sham, *Phys. Rev.* **140**, A1133 (1965).
24. P. Borlido, J. Schmidt, A. W. Huran, F. Tran, M. A. L. Marques, and S. Botti, *NPJ Comput. Mater.* **6**, 96 (2020).
25. J. P. Perdew, and A. Zunger, *Phys. Rev. B* **23**, 5048 (1981).
26. K.-H. Xue, J.-H. Yuan, L. R. C. Fonseca, and X.-S. Miao, *Comput. Mater. Sci.* **153**, 493 (2018).
27. A. I. Johnson, K. P. K. Withanage, K. Sharkas, Y. Yamamoto, T. Baruah, R. R. Zope, J. E. Peralta, and K. A. Jackson, *J. Chem. Phys.* **151**, 174106 (2019).
28. D. Hait, and M. Head-Gordon, *J. Phys. Chem. Lett.* **9**, 6280 (2018).
29. M. Li, R. Kobayashi, R. D. Amos, M. J. Ford, and J. R. Reimers, *Chem. Sci.* **13**, 1492 (2022).
30. M. Li, J. R. Reimers, M. J. Ford, R. Kobayashi, and R. D. Amos, *J. Comput. Chem.* **42**, 1486 (2021).
31. A. D. Becke, *J. Chem. Phys.* **98**, 5648 (1993).
32. P. J. Stephens, F. J. Devlin, C. F. Chabalowski, and M. J. Frisch, *J. Phys. Chem.* **98**, 11623 (1994).
33. C. Adamo, and V. Barone, *J. Chem. Phys.* **110**, 6158 (1999).
34. A. V. Krukau, O. A. Vydrov, A. F. Izmaylov, and G. E. Scuseria, *J. Chem. Phys.* **125**, 224106 (2006).
35. J. H. Skone, M. Govoni, and G. Galli, *Phys. Rev. B* **93**, 235106 (2016).
36. W. Chen, G. Miceli, G.-M. Rignanese, and A. Pasquarello, *Phys. Rev. Mater.* **2**, 073803 (2018).
37. P. Liu, C. Franchini, M. Marsman, and G. Kresse, *J. Phys.: Condens. Matter* **32**, 015502 (2019).
38. J. E. Moussa, P. A. Schultz, and J. R. Chelikowsky, *J. Chem. Phys.* **136**, 204117 (2012).
39. P. Borlido, T. Aull, A. W. Huran, F. Tran, M. A. L. Marques, and S. Botti, *J. Chem. Theory Comput.* **15**, 5069 (2019).
40. J. P. Perdew, K. Burke, and M. Ernzerhof, *Phys. Rev. Lett.* **77**, 3865 (1996).

41. L. Goerigk, and S. Grimme, *Phys. Chem. Chem. Phys.* **13**, 6670 (2011).
42. V. Coropceanu, X.-K. Chen, T. Wang, Z. Zheng, and J.-L. Brédas, *Nat. Rev. Mater.* **4**, 689 (2019).
43. M. P. Bircher, and U. Rothlisberger, *J. Chem. Theory Comput.* **14**, 3184 (2018).
44. S. E. Gant, J. B. Haber, M. R. Filip, F. Sagredo, D. Wing, G. Ohad, L. Kronik, and J. B. Neaton, *Phys. Rev. Mater.* **6**, 053802 (2022).
45. H. Iikura, T. Tsuneda, T. Yanai, and K. Hirao, *J. Chem. Phys.* **115**, 3540 (2001).
46. Y. Tawada, T. Tsuneda, S. Yanagisawa, T. Yanai, and K. Hirao, *J. Chem. Phys.* **120**, 8425 (2004).
47. T. Yanai, D. P. Tew, and N. C. Handy, *Chem. Phys. Lett.* **393**, 51 (2004).
48. R. Kobayashi, and R. D. Amos, *Chem. Phys. Lett.* **420**, 106 (2006).
49. Z.-L. Cai, M. J. Crossley, J. R. Reimers, R. Kobayashi, and R. D. Amos, *J. Phys. Chem. B* **110**, 15624 (2006).
50. J. R. Reimers, Z.-L. Cai, R. Kobayashi, M. Rätsep, A. Freiberg, and E. Krausz, *Sci. Rep.* **3**, 2761 (2013).
51. M. Rätsep, Z.-L. Cai, J. R. Reimers, and A. Freiberg, *J. Chem. Phys.* **134**, 024506 (2011).
52. S. Yin, M. G. Dahlbom, P. J. Canfield, N. S. Hush, R. Kobayashi, and J. R. Reimers, *J. Phys. Chem. B* **111**, 9923 (2007).
53. J. R. Reimers, A. Sajid, R. Kobayashi, and M. J. Ford, *J. Chem. Theory Comput.* **14**, 1602 (2018).
54. D. Golze, M. Dvorak, and P. Rinke, *Frontiers in Chemistry* **7** (2019).
55. M. Shao, L. Lin, C. Yang, F. Liu, F. H. Da Jornada, J. Deslippe, and S. G. Louie, *Sci. China Math.* **59**, 1593 (2016).
56. P. Rinke, A. Qteish, J. Neugebauer, C. Freysoldt, and M. Scheffler, *New J. Phys.* **7**, 126 (2005).
57. F. Fuchs, J. Furthmüller, F. Bechstedt, M. Shishkin, and G. Kresse, *Phys. Rev. B* **76**, 115109 (2007).
58. F. Bruneval, and M. A. L. Marques, *J. Chem. Theory Comput.* **9**, 324 (2013).
59. M. J. van Setten, F. Caruso, S. Sharifzadeh, X. Ren, M. Scheffler, F. Liu, J. Lischner, L. Lin, J. R. Deslippe, S. G. Louie, C. Yang, F. Weigend, J. B. Neaton, F. Evers, and P. Rinke, *J. Chem. Theory Comput.* **11**, 5665 (2015).
60. A. Rasmussen, T. Deilmann, and K. S. Thygesen, *NPJ Comput. Mater.* **7**, 22 (2021).
61. L. Zhang, Y. Shu, C. Xing, X. Chen, S. Sun, Y. Huang, and D. G. Truhlar, *J. Chem. Theory Comput.* **18**, 3523 (2022).
62. J. Sun, A. Ruzsinszky, and J. P. Perdew, *Phys. Rev. Lett.* **115**, 036402 (2015).
63. A. Sajid, J. R. Reimers, R. Kobayashi, and M. J. Ford, *Phys. Rev. B* **102**, 144104 (2020).
64. A. Sajid, M. J. Ford, and J. R. Reimers, *Rep. Prog. Phys.* **83**, 044501 (2020).
65. J. R. Reimers, J. Shen, M. Kianinia, C. Bradac, I. Aharonovich, M. J. Ford, and P. Piecuch, *Phys. Rev. B* **102**, 144105 (2020).
66. J. R. Reimers, A. Sajid, R. Kobayashi, and M. J. Ford, *J. Phys. Chem. C* **124**, 21178 (2020).
67. D. Wing, G. Ohad, J. B. Haber, M. R. Filip, S. E. Gant, J. B. Neaton, and L. Kronik, *Proc. Natl. Acad. Sci.* **118**, e2104556118 (2021).
68. S. Hastrup, M. Strange, M. Pandey, T. Deilmann, P. S. Schmidt, N. F. Hinsche, M. N. Gjerding, D. Torelli, P. M. Larsen, A. C. Riis-Jensen, J. Gath, K. W. Jacobsen, J. Jørgen

- Mortensen, T. Olsen, and K. S. Thygesen, *2D Mater.* **5**, 042002 (2018).
69. M. N. Gjerding, A. Taghizadeh, A. Rasmussen, S. Ali, F. Bertoldo, T. Deilmann, N. R. Knøsgaard, M. Kruse, A. H. Larsen, S. Manti, T. G. Pedersen, U. Petralanda, T. Skovhus, M. K. Svendsen, J. J. Mortensen, T. Olsen, and K. S. Thygesen, *2D Mater.* **8**, 044002 (2021).
70. M. Yao, Y. Wang, X. Li, Y. Sheng, H. Huo, L. Xi, J. Yang, and W. Zhang, *Sci. Data* **8**, 236 (2021).
71. G. Kresse, and J. Hafner, *Phys. Rev. B* **47**, 558 (1993).
72. G. Kresse, and J. Furthmüller, *Comput. Mat. Sci.* **6**, 15 (1996).
73. G. Kresse, and D. Joubert, *Phys. Rev. B* **59**, 1758 (1999).
74. W. Li, and F. Giustino, *Phys. Rev. B* **101**, 035201 (2020).

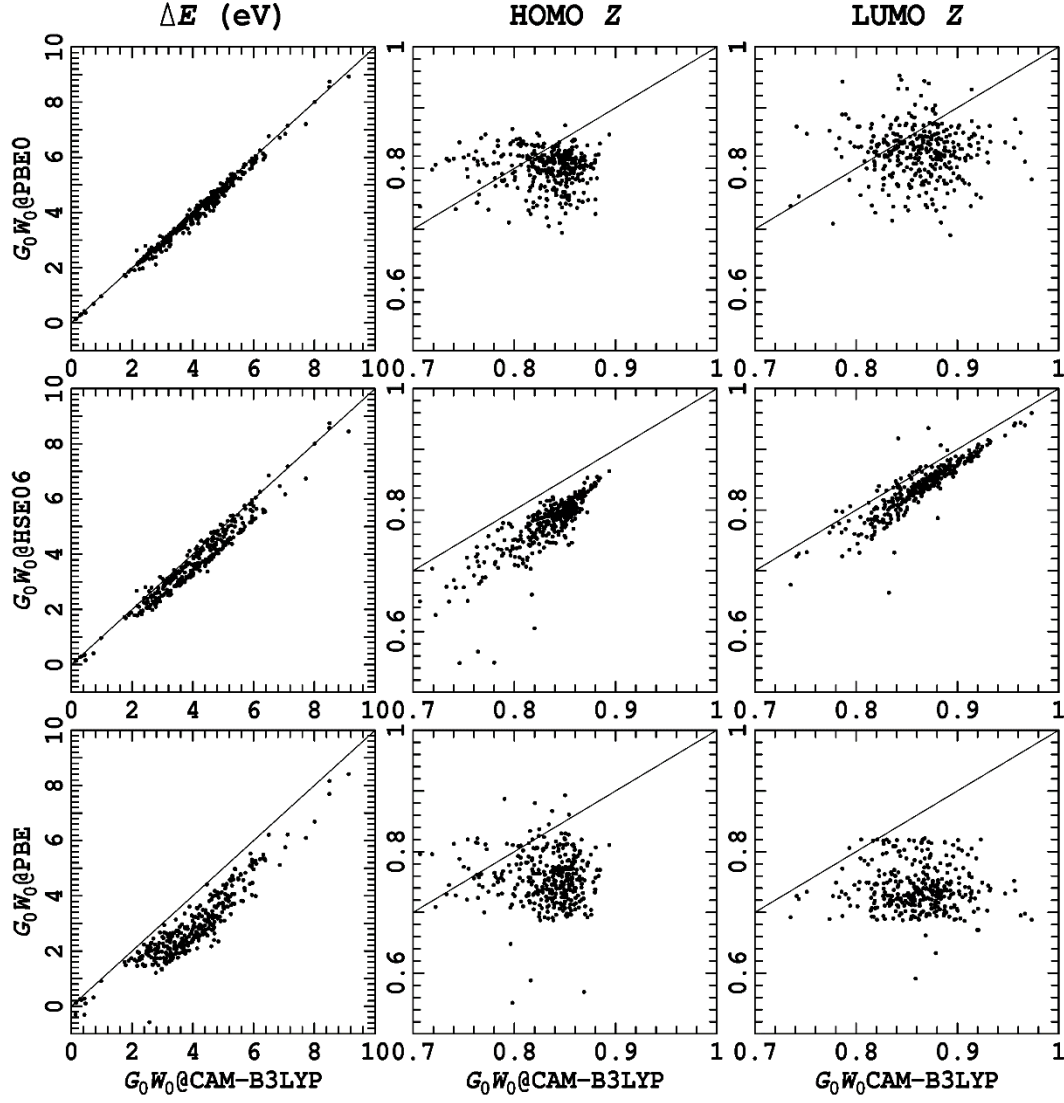


FIG 1. Correlation of the calculated bandgap, ΔE , and the quasiparticle weight Z for the HOMO and LUMO orbitals, for 341 2D materials, as calculated using $G_0W_0@HSE06$, $G_0W_0@PBE0$, and $G_0W_0@PBE$, with those calculated using $G_0W_0@CAM-B3LYP$.

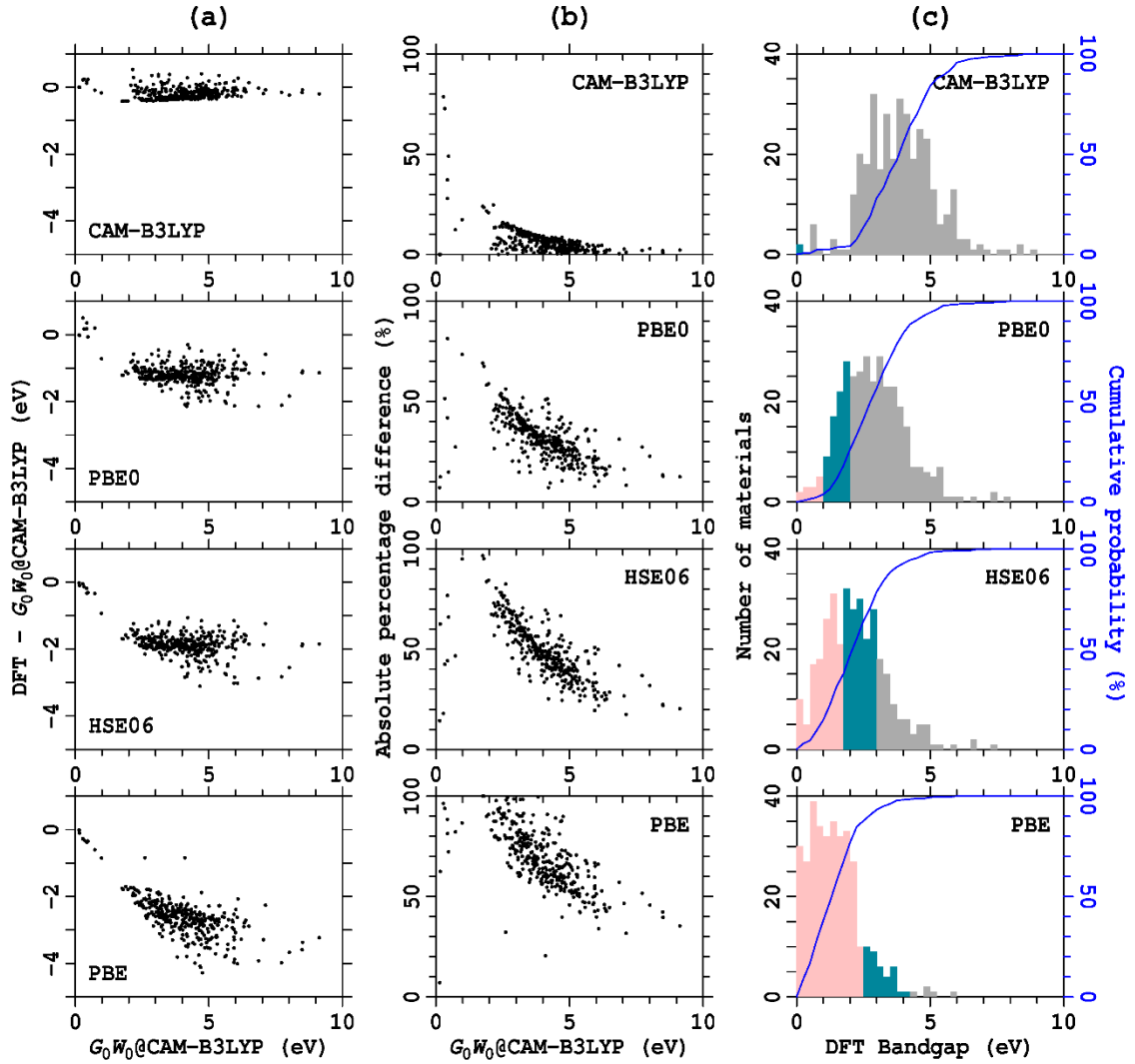


FIG 2. Bandgap analyses for DFT calculations. (a) the difference to $G_0W_0@CAM-B3LYP$ versus the $G_0W_0@CAM-B3LYP$ values. (b) Analogous percentage absolute deviations. (c) The number of materials predicted with different DFT bandgaps, and their cumulative probability distribution; grey colored regions are ones for which the DFT result can always be taken with confidence, whereas pink colored regions should be taken with caution if significant charge transfer is implicated. Analogous results versus $G_0W_0@HSE06$ are given in SM Fig. S1.

Table I. Comparison of calculated bandgaps of one type of calculation to another, listing the mean difference (MD), mean-absolute difference (MAD), the maximum absolute difference and the most-negative and most-positive differences, as well as the mean absolute percentage difference (MAPD).

to	of	MD (eV)	MAD (eV)	MAX Abs. (eV)	Most negative (eV)	Most positive (eV)	MAPD (%)
$G_0W_0@CAM-B3LYP$	$G_0W_0@PBE0$	-0.12	0.14	0.66	-0.66	0.47	4
	$G_0W_0@HSE06$	-0.36	0.39	1.11	-1.11	0.52	11
	$G_0W_0@PBE$	-1.11	1.11	3.15	-3.15	-0.03	30
	CAM-B3LYP	-0.19	0.23	0.53	-0.42	0.53	7
	PBE0	-1.17	1.19	2.14	-2.14	0.5	32
	HSE06	-1.84	1.84	3.11	-3.11	-0.02	49
	PBE	-2.61	2.61	4.28	-4.28	-0.01	67
$G_0W_0@PBE0$	PBE0	-1.06	1.07	2.09	-2.09	0.50	29
$G_0W_0@HSE06$	HSE06	-1.48	1.48	3.23	-3.23	0.00	42
$G_0W_0@PBE$	PBE	-1.50	1.51	3.38	-3.38	1.07	52

Table II. The quasiparticle weight (renormalization factor) Z for the initial DFT wavefunction in the final G_0W_0 wavefunction for the HOMO and LUMO bands.

Method	HOMO		LUMO	
	minimum	average	minimum	average
$G_0W_0@CAM-B3LYP$	0.71	0.83	0.74	0.86
$G_0W_0@PBE0$	0.69	0.83	0.69	0.80
$G_0W_0@HSE06$	0.55	0.78	0.66	0.84
$G_0W_0@PBE$	0.59	0.74	0.55	0.76

T52	C2/m	20m-3731	T52HC2_m20m-3731	2.25	0.77	1.40	0.05	2.63	2.44	2.60	1.77	0.790	0.832	0.811	0.750	0.814	0.782	0.781	0.756	0.77	0.887	0.728	0.807	-0.38	-1.85	-1.23	-2.58	-0.19	-1.67	-1.05	-2.40	-0.35	-1.83	-1.21	-2.56	0.48	-1.00	-0.38	-1.73	-0.19	-0.03	-0.86	0.03	-0.16	-0.83	
T2B2	P4/m	20m-5125	T2B2P4Pmm20m-5125	5.51	3.95	4.62	1.13	5.40	5.18	5.31	4.96	0.870	0.924	0.897	0.820	0.904	0.867	0.813	0.851	0.83	0.897	0.749	0.723	0.10	-1.45	-0.78	-2.27	0.31	-1.22	-0.56	-2.04	0.20	-1.35	-0.69	-2.18	0.55	-1.00	-0.34	-1.85	0.23	-0.10	-0.45	0.10	-0.13	-0.35	
T2C2	P4/m	20m-1112	T2C2P4P_mmm20m-1112	5.09	4.52	5.19	1.63	6.01	5.26	5.80	5.23	0.866	0.931	0.899	0.820	0.913	0.872	0.818	0.844	0.83	0.920	0.759	0.779	-0.02	-1.50	-0.82	-2.39	0.73	-0.75	-0.07	-1.64	0.19	-1.29	-0.61	-2.18	0.76	-0.71	-0.04	-1.60	0.75	-0.21	-0.78	0.21	-0.54	-0.37	
T2F2	P4/m	20m-3772	T2F2P4P_mmm20m-3772	6.29	4.64	5.34	1.61	6.36	5.57	5.99	5.35	0.851	0.929	0.890	0.793	0.907	0.850	0.815	0.826	0.82	0.925	0.793	0.714	-0.08	-1.72	-1.03	-2.75	0.71	-0.93	-0.24	-1.96	0.29	-1.35	-0.66	-2.38	0.94	-0.71	-0.01	-1.74	-0.79	-0.37	-1.02	0.37	-0.42	-0.64	
T2D2	P4/m	20m-3762	T2D2P4Pmm20m-3762	5.12	3.56	4.22	2.84	4.72	4.22	4.62	4.18	0.869	0.913	0.891	0.822	0.888	0.855	0.760	0.788	0.75	0.723	0.724	0.723	0.40	-1.15	-0.49	-1.88	0.90	-0.65	0.01	-1.38	0.50	-1.05	-0.39	-1.78	0.94	-0.62	0.05	-1.34	0.50	-1.00	-0.54	0.10	-0.40	-0.44	
T2D	Cm	20m-4083	T2DHCm20m-4083	3.76	2.09	2.72	1.49	3.88	3.24	3.26	2.02	0.829	0.894	0.861	0.788	0.860	0.799	0.805	0.801	0.80	0.767	0.749	0.758	-0.12	-1.79	-1.17	-2.39	0.53	-1.15	-0.52	-1.74	0.50	-1.17	-0.54	-1.77	1.74	0.07	0.69	-0.53	-0.65	-0.62	-1.86	0.62	-0.02	-1.24	
T2D3	C2	20m-836	T2D3C2m20m-836	3.42	1.95	2.65	0.93	3.74	3.06	3.46	2.86	0.765	0.849	0.807	0.679	0.796	0.717	0.757	0.737	0.75	0.758	0.702	0.730	-0.32	-1.79	-1.09	-2.81	0.36	-1.11	-0.41	-2.13	-0.04	-1.50	-0.80	-2.53	0.56	-0.91	-0.21	-1.93	-0.68	-0.28	-0.88	0.28	0.40	-1.60	
T2D3	P1	20m-2066	T2D3P1m20m-2066	3.91	1.77	2.48	0.80	4.23	4.02	4.22	2.56	0.767	0.827	0.812	0.683	0.829	0.756	0.850	0.872	0.86	0.763	0.743	0.743	-0.32	-2.45	-1.75	-3.63	0.11	-2.04	-1.04	-3.22	-0.31	-2.45	-1.74	-3.62	1.35	-0.78	0.08	1.78	0.21	-0.01	-1.67	0.01	-0.20	-1.66	
T2D3	P1	20m-3783	T2D3P1m20m-3783	2.94	1.45	2.13	0.64	3.31	3.23	3.27	1.69	0.770	0.783	0.805	0.714	0.826	0.770	0.808	0.856	0.83	0.700	0.760	0.730	-0.38	-1.86	-1.18	-2.67	-0.29	-1.77	-1.10	-2.59	0.34	-1.82	-1.14	-2.63	1.24	-0.24	0.43	1.06	0.08	-0.04	-1.62	0.04	-0.04	-1.58	
T2S2	P1	20m-2963	T2S2P1m20m-2963	3.12	1.73	2.38	1.09	3.68	3.05	3.26	1.99	0.847	0.869	0.858	0.780	0.859	0.820	0.756	0.780	0.76	0.748	0.739	0.743	-0.36	-1.95	-1.30	-2.59	0.26	-1.32	-0.67	-1.96	0.56	-1.53	-0.88	-2.16	1.33	-0.26	0.39	0.90	-0.63	-0.41	-1.69	0.41	-0.20	-1.37	
T2S2	P1	20m-1404	T2S2P1m20m-1404	2.78	1.36	2.00	0.77	3.15	3.01	3.08	1.86	0.823	0.857	0.840	0.777	0.825	0.801	0.801	0.831	0.82	0.734	0.748	0.741	-0.16	-1.79	-1.15	-2.37	-0.23	-1.65	-1.01	-2.23	-0.30	-1.72	-1.08	-2.30	0.92	-0.50	0.14	1.09	0.14	-0.07	-1.29	0.07	-0.07	-1.22	
T2S3	P1	20m-1880	T2S3P1m20m-1880	3.83	1.47	2.11	0.73	3.99	3.34	3.88	3.10	0.838	0.871	0.854	0.756	0.835	0.795	0.836	0.852	0.84	0.759	0.804	0.781	-0.17	-2.53	-1.88	-3.26	0.50	-1.87	-1.23	-2.61	0.04	-2.41	-1.77	-3.15	0.73	-1.64	-0.99	-2.37	0.66	-0.12	-0.89	0.12	-0.54	-0.77	
T2S5	P1	20m-665	T2S5P1m20m-665	2.82	1.35	2.00	0.75	2.89	2.62	2.84	2.29	0.837	0.871	0.855	0.775	0.835	0.805	0.837	0.839	0.83	0.746	0.722	0.734	-0.07	-1.54	-0.89	-2.14	0.20	-1.27	-0.62	-1.87	-0.02	-1.49	-0.84	-2.09	0.52	-0.95	-0.29	-1.55	0.26	-0.55	-0.59	0.05	-0.21	-0.54	
T2S62	Cm	20m-729	T2S62Cm20m-729	2.46	1.08	1.69	0.59	2.86	2.79	2.85	1.49	0.832	0.862	0.847	0.776	0.828	0.802	0.808	0.829	0.82	0.744	0.754	0.749	-0.40	-1.78	-1.17	-2.27	-0.33	-1.71	-1.10	-2.20	-0.39	-1.76	-1.16	-2.26	0.39	-0.77	-0.41	0.20	0.90	-0.07	-0.01	-0.37	0.01	-0.06	-1.36
T2S62	Pm	20m-2962	T2S62Pm20m-2962	2.63	1.08	1.70	0.55	3.02	2.75	2.95	2.27	0.849	0.853	0.851	0.774	0.857	0.816	0.808	0.818	0.81	0.725	0.714	0.720	-0.39	-1.94	-1.32	-2.47	-0.12	-1.67	-1.05	-2.20	-0.33	-1.87	-1.25	-2.40	0.35	-1.19	-0.57	-1.72	-0.27	-0.07	-0.75	0.07	-0.20	-0.68	
T2S63	P1	20m-1024	T2S63P1m20m-1024	2.11	0.82	1.40	0.23	2.50	2.39	2.50	2.17	0.844	0.866	0.855	0.759	0.838	0.799	0.776	0.778	0.78	0.804	0.702	0.753	-0.40	-1.69	-1.10	-2.27	-0.28	-1.57	-0.99	-2.16	-0.39	-1.68	-1.10	-2.27	0.06	-1.35	-0.77	-1.94	-0.12	-0.01	-0.33	0.01	-0.11	-0.31	
T2S65	P1	20m-231	T2S65P1m20m-231	2.76	1.15	1.78	0.57	3.11	2.94	3.04	1.65	0.839	0.874	0.857	0.768	0.839	0.804	0.787	0.790	0.79	0.807	0.814	0.810	-0.35	-1.96	-1.31	-2.55	0.18	-1.79	-1.16	-2.37	-0.29	-1.89	-1.27	-2.48	1.11	-0.30	0.13	1.08	0.17	0.07	-1.46	0.07	-0.10	-1.19	
T2T62	Cm	20m-1104	T2T62Cm20m-1104	2.29	0.97	1.54	0.55	2.65	2.51	2.60	2.01	0.838	0.865	0.851	0.769	0.833	0.796	0.817	0.813	0.83	0.745	0.732	0.739	-0.36	-1.68	-1.11	-2.10	-0.22	-1.54	-0.97	-1.96	-0.11	-1.63	-1.06	-2.05	0.28	-1.04	-0.48	-1.47	0.14	-0.05	-0.63	0.05	-0.09	-0.59	
T2T63	P1	20m-1315	T2T63P1m20m-1315	0.59	0.10	0.61	0.09	0.43	0.36	0.43	0.28	0.850	0.865	0.857	0.758	0.827	0.792	0.717	0.837	0.83	0.715	0.814	0.764	-0.16	-0.33	-0.18	-0.35	0.23	-0.26	-0.25	-0.28	0.16	-0.33	0.18	-0.34	0.32	-0.18	0.33	-0.19	-0.07	0.00	-0.15	0.07	-0.07	-0.15	
T2T65	P1	20m-1621	T2T65P1m20m-1621	2.80	1.10	1.83	0.54	3.15	2.98	3.13	2.37	0.851	0.881	0.866	0.776	0.845	0.810	0.799	0.815	0.80	0.812	0.740	0.776	-0.36	-2.10	-1.33	-2.62	-0.18	-1.93	-1.35	-2.44	-0.33	-2.08	-1.50	-2.60	0.43	-1.32	-0.75	-1.84	-0.17	-0.02	-0.78	0.02	-0.15	-0.76	
T2S2	P1	20m-3849	T2S2P1m20m-3849	4.24	2.61	3.27	1.90	4.53	3.82	4.49	3.25	0.813	0.888	0.860	0.791	0.867	0.829	0.813	0.807	0.81	0.701	0.816	0.758	-0.29	-1.92	-1.26	-2.63	0.42	-1.21	-0.55	-1.92	-0.25	-1.88	-1.22	-2.59	0.99	-0.64	0.02	1.35	0.71	-0.04	-1.28	0.04	-0.67	-1.24	
UC2F2	P2/m	20m-5199	UC2F2P2_m20m-5199	5.13	3.56	4.30	2.09	5.30	4.82	5.09	4.72	0.755	0.774	0.764	0.705	0.763	0.734	0.822	0.862	0.84	0.772	0.889	0.731	-0.17	-1.74	-1.00	-3.21	0.32	-1.26	-0.52	-2.73	0.05	-1.53	-0.79	-3.00	0.41	-1.16	-0.42	-2.63	0.48	0.21	-0.58	0.21	-0.27	-0.37	
VF5	Pmm	20m-2503	VF5Pmm20m-2503	2.61	1.44	2.11	0.28	3.28	3.54	3.59	2.54	0.719	0.743	0.730	0.704	0.714	0.714	0.786	0.869	0.83	0.796	0.727	0.761	-0.37	-1.84	-1.16	-3.00	0.37	-1.11	-0.43	-2.37	-0.28	-1.75	-1.08	-2.91	0.37	-1.10	-0.43	-2.36	0.73	-0.09	-0.74	0.09	0.65	0.65	
W2N2	P-1	20m-2568	W2N2P-1m20m-2568	0.50	0.23	0.28	0.01	0.28	0.27	0.28	0.25	0.826	0.841	0.833	0.812	0.842	0.827	0.792	0.820	0.81	0.783	0.730	0.756	0.22	0.05	0.50	0.27	0.23	-0.04	0.11	-0.26	0.22	0.05	0.50	-0.27	0.25	-0.02	0.33	0.24	0.01	0.00	-0.03	0.01	-0.02		
W564	Pm	20m-391	W564Pm20m-391	0.65	0.39	0.59	0.13	0.73	0.61	0.69	0.32	0.888	0.855	0.846	0.821	0.852	0.836	0.765	0.769	0.77	0.759	0.712	0.735	-0.09	-0.34	0.20	-0.60	0.21	-0.02	0.52	-0.28	-0.05	-0.30	0.24	-0.56	0.33	0.07	0.61	-0.38	-0.32	-0.04	-0.41	0.04	-0.23	-0.38	
W2F2	Amn2	20m-4828	W2F2Amn2m20m-4828	4.06	2.44	3.14	1.35	4.13	3.58	4.09	3.56	0.788	0.859	0.823	0.770	0.841	0.806	0.790	0.808	0.778	0.743	0.748	-0.07	-1.69	-0.99	-2.78	0.48	-1.14	-0.44	-2.22	-0.01	-1.66	-0.95	-2.74	0.50	-1.12	-0.42	-2.21	0.55	-0.04	-0.57	0.04	-0.52	-0.53		
W03	Pm	20m-605	W03Pm20m-605	3.58	1.97	2.68	0.80	3.44	3.15	3.32	1.14	0.789	0.862	0.825	0.779	0.847	0.813	0.779	0.817	0.80	0.768	0.688	0.728	0.14	-1.47	-0.77	-2.64	0.43	-1.18	-0.47	-2.35	0.26	-1.35	-0.64	-2.52	0.44	-1.18	-0.47	-2.34	0.30	-0.13	-0.30	0.13	-0.17	-0.17	
W52	Amn2	20m-3749	W52Amn2m20m-3749	4.31	2.64	3.33	2.09	4.66	4.62	4.65	2.95	0.838	0.844	0.841	0.818	0.835	0.826	0.819	0.842	0.83	0.687	0.793	0.740	-0.35	-2.03	-1.32	-2.56	-0.32	-1.98	-1.29	-2.53	-0.35	-2.01	-1.32	-2.56	1.36	-0.30	0.39	-0.85	-0.03	0.00	-1.71	0.00	-0.03	-1.71	
W562	Amn2																																													